Research Square

Preprints are preliminary reports that have not undergone peer review.
They should not be considered conclusive, used to inform clinical practice,
or referenced by the media as validated information.

Synergistic Convergence of Multiple Environmental Drivers Triggered a Multi-taxa Regime Shift in the Yangtze Estuary

Hao Huang

huanghao@tio.org.cn

Third Institute of Oceanography, MNR

Danyun Ou

Third Institute of Oceanography, MNR

Yue Ni

Third Institute of Oceanography, MNR

Xiangwen Bao

Third Institute of Oceanography, MNR

Ming Chen

Third Institute of Oceanography, MNR

Weiwen Li

Lei Wang

Third Institute of Oceanography, Ministry of Natural Resources P.R.C. https://orcid.org/0000-0002-1279-5782

Article

Keywords: regime shift, threshold, multi-taxa; DO, DIN, phosphate, nutrient stoichiometry, Yangtze Estuary

Posted Date: August 20th, 2026

DOI: https://doi.org/10.21203/rs.3.rs-10591236/v1

License: This work is licensed under a Creative Commons Attribution 4.0 International License.
Read Full License

Additional Declarations: There is **NO** Competing Interest.

Synergistic Convergence of Multiple Environmental Drivers Triggered a Multi-taxa Regime Shift in the Yangtze Estuary

Abstract

Understanding regime shifts in large estuaries requires integrating long-term biological and environmental evidence. Here we showed that the Yangtze Estuary ecosystem underwent a fundamental reorganization centered on 2009–2010, based on two decades of summer data from four biotic groups and eight environmental variables. The ecosystem state (PC1) shifted from a stable negative regime to a highly variable state, corroborated by synchronous biodiversity declines and dominant species turnover across all trophic levels. We identified critical thresholds for dissolved oxygen, dissolved inorganic nitrogen, phosphate, and the nitrogen-to-phosphorus ratio. During 2007–2010, coordinated directional changes in these four drivers, rather than any single factor crossing an absolute threshold, drove the ecosystem transition. These thresholds mark the ranges where directional environmental trends, including nutrient imbalance alleviation and oxygen stress intensification, govern state changes rather than absolute concentrations. Our findings provide empirically grounded reference points for threshold-based management in the Yangtze Estuary.

Keywords

regime shift; threshold; multi-taxa; DO; DIN; phosphate; nutrient stoichiometry; Yangtze Estuary

Introduction

Estuarine and coastal ecosystems rank among the most productive environments, providing essential habitats for a wide range of plankton, fish, and benthic organisms that hold considerable commercial and ecological importance[1,2]. However, these systems are particularly vulnerable to destabilization due to their position at the land-sea interface, where natural hydrodynamics including tidal currents, seasonal freshwater pulses, and storm surges create inherent environmental variability[3,4]. Cumulative anthropogenic pressures such as coastal urbanization, watershed modifications, nutrient over-enrichment, and climate change, often exceed the adaptive capacity of keystone species, eroding ecosystem resilience through trophic cascades[5,6].

The rapid, persistent reorganizations of ecosystem structure and function, which was termed as ecological regime shifts, has gained prominence as a framework for understanding non-linear changes in marine and coastal systems[7]. Regime shifts are characterized by abrupt transitions from one relatively stable community state to another, often driven by the crossing of critical environmental thresholds[8]. In complex ecosystems such as marginal seas, estuaries, coastal areas, and lakes, the detection of regime shifts requires the integration of multi-taxa observations and robust analytical frameworks capable of capturing coherent patterns of change across biological groups[9-11]. This concept forms the scientific basis for interpreting contemporary ecosystem responses to perturbations while enabling predictive insights into future ecological trajectories[3,12].

A variety of statistical approaches have been developed to detect regime shifts from ecological time series[13]. Principal component analysis (PCA) has been widely employed to reduce high-dimensional community data to a few composite variables, and PC1-based trajectory analysis has proven effective in identifying regime shifts in diverse systems including the North Sea, the German Bight, and the North Pacific[8,11,14,15]. To enhance the robustness of breakpoint identification, multi-method consensus approaches combining PELT change point detection, Ba-Perron structural change tests, sliding-window analyses, and UPGMA clustering algorithms have been increasingly adopted[9,16]. This multi-method cross validation approach has been successfully applied in studies of regime shifts in lakes, marine

ecosystems, and forests, demonstrating its effectiveness in detecting the timing and direction of abrupt ecological transitions[10,15]. Additionally, distance-based redundancy analysis (db-RDA) has been used to quantify the relative contributions of environmental drivers to community variation[17], while threshold analysis methods including non-parametric derivative estimation, GAM-based permutation tests, and the exploratory SiZer method have been employed to identify critical ecological thresholds along environmental gradients[18-20]. The integration of these complementary analytical tools enables a more comprehensive understanding of both the timing of regime shifts and their underlying environmental mechanisms[21].

The Yangtze Estuary, one of the largest river-dominated estuaries worldwide, has experienced profound environmental changes over recent decades[22,23]. Escalating anthropogenic pressures including nutrient over-enrichment, dam induced alterations to material fluxes, and climate warming, have significantly modified the estuary's physical and chemical environment[24,25]. These changes have driven a series of ecological responses, including shifts in nutrient stoichiometry, expansion of hypoxic zones, and restructuring of phytoplankton communities from siliceous to non siliceous dominated assemblages[26,27]. Despite these well-documented environmental shifts, regime shift research in the Yangtze Estuary has largely focused on single biotic groups or individual environmental drivers, leaving the ecosystem wide response to multi-factor forcing insufficiently understood[28,29]. Most existing studies have examined phytoplankton community responses to nutrient changes, fish assemblage shifts following dam construction, or hypoxia dynamics in isolation[30-32]. Consequently, critical questions regarding whether the Yangtze Estuary has undergone a multi-taxa regime shift, what environmental thresholds are associated with such a transition, and how multiple drivers interact to push the ecosystem across a tipping point remain inadequately addressed.

Here we address these questions by synthesizing a 20 year summer monitoring dataset encompassing four biotic groups including phytoplankton, zooplankton, nekton, and benthos, alongside eight environmental variables derived from integrated in-situ measurements and satellite-based reanalysis products in the Yangtze Estuary. We employ a multi-method analytical framework combining PCA-based ecosystem state characterization, multi-method

breakpoint detection, clustering validation, and threshold analysis. Specifically, the study seeks to ascertain whether a multi-taxa regime shift occurred in the Yangtze Estuary during the study period, to pinpoint the environmental factors and their critical thresholds associated with the transition, and to elucidate the mechanisms through which the convergence of multiple environmental trends drove the ecosystem across a tipping point and fundamentally reorganized community structure across trophic levels.

Results

1 Biological Community Composition and Diversity in the Yangtze Estuary

From 2004 to 2023, the total number of species recorded in the Yangtze Estuary amounted to 540 for phytoplankton, 596 for zooplankton, 571 for benthos, and 273 for nekton. Among these, summer datasets were the most complete across all four taxonomic groups, comprising 466, 545, 488, and 224 species, respectively. Accordingly, all subsequent analyses were primarily based on summer data.

Inter-annual trends in diversity and richness indices revealed a sharp decline across all biotic groups during 2009–2010 (Fig.1a & b). Phytoplankton diversity reached its lowest value in 2009 (0.51±0.61), while species richness fell from 25.42±6.67 in 2008 to 11.79±7.52 in 2009, experiencing a reduction of 54%. Although richness began a gradual recovery from 2010, reaching 34.33±15.79 in 2011, the diversity index remained low at 0.91, suggesting a proliferation of low-abundance phytoplankton species and a persistently uneven community structure. Subsequent years exhibited strong fluctuations, with diversity dipping again in 2016 to 0.53±0.41 before recovering to 1.51±0.64 in 2022 and 1.56±0.60 in 2023. Richness showed no sustained directional trend but remained highly variable, ranging from 11.8 to 34.3 without a clear recovery trend (Fig. 1a & b).

Zooplankton communities followed a similar trajectory. Diversity and richness peaked in 2008 at 2.55±0.55 and 41.43±23.49 respectively, then dropped sharply in 2010 to 1.77±0.60 and 14.00±4.24 respectively. Over the following decade, zooplankton diversity fluctuated between 1.5 and 2.1, and despite occasional moderate increases, it never recovered to the pre-decline peak observed in 2008 (Fig. 1a). Richness displayed pronounced variability but never approached the 2008 maximum, averaging around 25 to 30 in recent years (Fig. 1b).

Benthic and nekton datasets were comparatively sparse, precluding robust trend analysis. Nonetheless, nekton diversity showed a decline from 2.60 ± 0.04 in 2007 to 1.01 ± 0.52 in 2017 and 1.51 ± 0.57 in 2023, suggesting a possible long-term decrease. Benthic diversity peaked in 2015 and 2016 with value of 2.08 ± 1.12 and 2.16 ± 0.84 respectively, but subsequently declined to low levels in recent years (Fig. 1a).

The synchronous collapse of diversity and richness across multiple taxonomic groups, particularly in phytoplankton and zooplankton, followed by only partial and inconsistent recovery, points to a fundamental reorganization of community structure during 2009–2010 that persisted in subsequent years.

2 Historical Physico-Chemical Conditions and Nutrient Dynamics

Physico-chemical variables were assembled from three complementary sources, namely in-situ measurements from the National Marine Data and Information Service (NMDIS), satellite-derived reanalysis products from the Copernicus Marine Service (CMEMS), and the gridded dataset of Lin et al. (2023), with their source composition varying by variable. Sea surface temperature (SST) and pH were derived exclusively from CMEMS products, as no concurrent in-situ measurements were available. Dissolved oxygen (DO), dissolved inorganic nitrogen (DIN), and phosphate were each supported by all three sources, with the Lin dataset providing additional spatial coverage for these nutrients. Salinity and chlorophyll *a* (Chl *a*) combined CMEMS satellite data with NMDIS in-situ measurements. Cross-validation between satellite-derived and in-situ data was conducted for variables with both data types available, including DO, DIN, phosphate, salinity, and Chl *a*, showing consistent seasonal and inter-annual patterns (Figs. S1a-e). For SST and pH, only satellite data were available and were used directly without in-situ validation. The N/P ratio was calculated from the DIN and phosphate concentrations. For each variable, summer means from 2004 to 2023 were calculated by averaging all available observations across June, July, and August, as shown in Figures 2a–h.

SST exhibited a fluctuating upward trend, rising from 25.13°C in 2004 to a peak of 29.46°C in 2010, then dropping to 26.25°C in 2011 before oscillating between 26.25 and 28.70°C. The 20-year mean was 27.43°C (Fig. 2a). DO declined steadily over the study period, from 7.64 mg/L in 2004 to 7.20 mg/L in 2023, with an anomalous low of 6.50 mg/L recorded in 2010 and extended lows below 6.50 mg/L in 2017 and 2020. The 20-year average was 7.04 mg/L, although the post-2010 mean was substantially lower than the pre-2010 average (Fig. 2b). Salinity exhibited extreme inter-annual variability, with values ranging from 28 to 31 psu during 2004 through 2009, then dropping anomalously to 3.24 psu in 2010.

Additional low salinity episodes occurred in 2014 and 2015, with values of 18.04 and 16.22 psu respectively, while from 2017 to 2023 salinity fluctuated between 23 and 26 psu. These low salinity events primarily reflected the proximity of sampling sites to the coast, making them susceptible to substantial riverine freshwater input. The 20-year mean, including anomalous year, was 25.20 psu (Fig. 2c). pH varied within a narrow range from 7.96 to 8.06, with a 20-year mean of 8.02 (Fig. 2d). Chl *a* concentrations fluctuated considerably over the study period, starting at 4.40 μg/L in 2004, reaching a minimum of 0.47 μg/L in 2010, recovering to 2.30 μg/L in 2012, and ranging between 3.22 and 4.10 μg/L from 2022 to 2023. The 20-year mean was 3.41 μg/L (Fig. 2e).

DIN concentrations showed pronounced fluctuations, peaking at 3.14 mg/L in 2007, declining after 2009 to 0.83 mg/L in 2011, and generally ranging between 0.5 and 1.0 mg/L after 2015. The overall mean was 1.38 mg/L (Fig. 2f). Phosphate concentrations ranged from 0.010 to 0.038 mg/L, with a notable peak of 0.038 mg/L in 2010, and a 20-year mean of 0.024 mg/L (Fig. 2g). The N/P ratio, calculated from DIN and phosphate concentrations, exhibited extreme inter-annual variability, reaching a high of 177 in 2004, declining to 80 in 2009 and 39 in 2010, and generally remaining between 20 and 40 after 2015. The 20-year mean was 73.2, which was strongly influenced by the exceptionally high values recorded in the early years of the record (Fig. 2h).

A closer examination of the 2007–2010 window revealed a distinct pattern of coordinated directional changes across multiple variables. While SST rose sharply to its record high in 2010 and salinity plummeted to its minimum, the most ecologically relevant shifts occurred in the nutrient and oxygen regimes. DO declined from 7.67 mg/L in 2007 to 7.09 mg/L in 2009 and further to 6.50 mg/L in 2010. DIN decreased from 3.14 mg/L in 2007 to 1.65 mg/L in 2009 and to 1.48 mg/L in 2010, a reduction of more than 50% over three years. Concurrently, phosphate rose from 0.015 mg/L in 2008 to 0.020 mg/L in 2009 and reached 0.038 mg/L in 2010, an increase of more than 150% over the same period. The N/P ratio declined correspondingly from 144 in 2008 to 80 in 2009 and to 39 in 2010. These synchronous changes, with DIN and N/P decreasing while phosphate increased and DO declined, represent a fundamental shift in nutrient and oxygen regimes in the Yangtze Estuary during this period.

3 Temporal heterogeneity of environmental drivers revealed by year-specific dbRDA

The overall influence of environmental variables on the inter-annual variability of community composition across the four biotic groups was assessed using distance-based redundancy analysis (dbRDA). The constrained model explained 22.8% of the total variation, and among the eight variables examined, only dissolved oxygen (DO) emerged as a statistically significant driver ($F = 2.436$, $p = 0.008$), suggesting that DO was the predominant long-term regulator of community variation in the Yangtze Estuary (Fig. 3a).

Year-specific dbRDA analyses, however, revealed pronounced temporal heterogeneity in the identity and number of significant environmental drivers, with a clear contrast between the pre-shift and post-shift periods. During 2004–2008, significant factors were detected only in 2006 and 2007, with combinations of SST, DO, salinity, and N/P ratio emerging as significant drivers. From 2009 to 2010, however, the number of significant drivers dropped sharply. In 2009, only NP ratio emerged as a significant driver ($p = 0.004$), while in 2010 analyzed with a simplified DO + SST model due to limited sample size, neither DO nor SST was significant, reflecting a temporary breakdown of the previously established environmental and community coupling during this period. From 2011 to 2018, the number of significant factors remained variable and relatively low. Most years showed only one or two significant drivers, with SST in 2011 and 2014, SST and DO in 2013, DIN, salinity, and N/P ratio in 2016, and DO, phosphate, Chl *a*, and N/P ratio in 2017. Years such as 2012, 2015, and 2018 exhibited no significant factors at all, implying a prolonged period of weakened environmental control over community composition. From 2019 onward, however, the number of significant factors increased markedly. In 2021 and 2022, nearly all eight environmental variables became significant simultaneously, and in 2023, all variables including N/P ratio were significant, indicating a transition toward strong multi-factor regulation of community structure (Fig. 3b).

SST and DO were the most consistently significant factors across the entire time series, underscoring their role as core long-term regulators (Figs. 3b). DIN and phosphate exerted strong influence in specific years, including 2006, 2016, and 2017, and years after 2019, while salinity effects were more sporadic, appearing mainly in 2006, 2007, 2016, and after

2020, likely reflecting inter-annual variability in riverine discharge. Collectively, these results reveal a clear temporal pattern in environmental forcing, that is, moderate multi-factor control during the early period (2004–2008), a transient loss of significant drivers during 2009–2010, a prolonged phase of reduced environmental coupling (2011–2018), and a subsequent return to strong multi-factor regulation from 2019 onward (Fig. 3). This temporal heterogeneity underscores the non-stationary nature of community and environment relationships and provides a basis for identifying potential structural changes in the ecosystem.

4 Identification of Regime Shifts in the Yangtze Estuary Ecosystem

As an objective integrative variable derived from PCA based on multi-taxa biological data including phytoplankton, zooplankton, nekton, and benthos, PC1 captured the most prominent signal of variation in the high-dimensional ecological community matrix, thereby maximally representing the coherent patterns of change across diverse biological groups. For the summer ecosystem of the Yangtze Estuary, PC1 explained 41.57% of the total variance of 1642 species, indicating that it effectively condenses the major synoptic variability in community composition (Fig. S2a). Analysis of the PC1 time series (2004–2023) using three independent breakpoint detection methods, PELT, strucchange, and a sliding-window bootstrap test, revealed a consensus breakpoint in 2009 (Fig S2b). The sliding-window method identified only 2009, strucchange additionally detected breakpoints in 2018 and 2020, while PELT did not detect any breakpoints (Fig. S2b).

To further validate this statistical breakpoint, we performed hierarchical clustering using Bray-Curtis distance and the UPGMA method on the multi-taxa community matrix. Silhouette analysis identified an optimal cluster number of k = 2 (Fig. S3a), and the temporal trajectory of cluster membership revealed that the system shifted between these two states multiple times (Fig. S3b). The system shifted from Cluster 1 to Cluster 2 during the period of 2009 to 2010, then returned to Cluster 1 from 2010 to 2011, followed by another shift from Cluster 1 to Cluster 2 between 2018 and 2019, and finally a shift from Cluster 2 back to Cluster 1 from 2020 to 2021 (Fig. S3b). Cross-validation between the PC1-derived consensus breakpoint and the cluster shifts confirmed 2009–2010 as the definitive regime-shift period, representing the most substantial structural reorganization of the ecosystem, when PC1 shifted

from a stable negative regime to a highly variable state (Fig. 4). Importantly, separate PCA performed on each individual biotic group yielded divergent PC1 temporal patterns and inconsistent breakpoints across groups (Figs. S4a–d), precluding a consensus regime-shift year. This finding underscored that when assessing ecosystem-wide regime shifts, using the combined community composition of all biotic groups as the analytical baseline offered a more comprehensive and robust reflection of changes in ecosystem stability.

Prior to the shift, from 2004 to 2008, PC1 values were consistently negative, ranging from -0.30 to -0.19, indicating a relatively stable community state dominated by a particular compositional configuration corresponding to Cluster 1. After 2009, the PC1 trajectory exhibited a marked transformation, as the index became highly variable with pronounced positive excursions. The shift from 2009 to 2010 saw PC1 rise from -0.26 to 0.71, an increase of nearly one unit, representing the first and most fundamental departure from the pre-shift negative regime (Fig. 4). Subsequent fluctuations, including the decline from 0.71 in 2010 to -0.26 in 2011 and the rises to 0.82 in 2019 and 0.79 in 2020, exhibited comparable or even greater amplitudes. However, these excursions occurred within a post-shift regime that had already been fundamentally reorganized, whereas the 2009–2010 transition represented the initial crossing from a long-established stable state into a new dynamic regime. The system shifted from a narrow negative range to a wide-amplitude fluctuating regime, indicating a fundamental reorganization of community structure (Fig. 4). The post-shift period was characterized by the multiple cluster changes after 2009, including the shifts from 2010 to 2011, from 2018 to 2019, and from 2020 to 2021 (Fig. S3b). This pattern suggested that the ecosystem did not settle into a single new stable state but rather entered a dynamic regime with recurrent compositional shifts, highlighting the loss of previous stability and the increased susceptibility to environmental forcing. Collectively, the convergence of PC1-based breakpoint detection and clustering evidence delineates the 2009–2010 interval as the critical regime-shift window. Over this period, PC1 shifted from a low-variance, persistently negative state to a high-variance, multi-modal pattern, while the cluster analysis recorded the first and pronounced transition from Cluster 1 to Cluster 2, together indicating a fundamental biological reorganization of the Yangtze Estuary summer ecosystem (Fig. 4).

5 Dominant Species Turnover Before and After the Regime Shift

To further corroborate the ecological reality of the 2009 regime shift, we examined changes in dominant species composition across the four biotic groups using data from the full 2004–2023 time series (Fig. 5). The dominant species turnover across all groups revealed a coherent pattern of community restructuring centered around the 2009–2010 period.

Phytoplankton exhibited a clear transition from a single-species diatom dominance to a more diversified diatom assemblage with increasing dinoflagellate representation. Before 2009, *Skeletonema costatum* overwhelmingly dominated the community, accounting for 56.7% to 85.0% of total abundance. In 2009, *S. costatum* still maintained its dominance at 65.0%. A pronounced shift occurred in 2010, when *S. costatum* plummeted to 13.1% and was replaced by a suite of new dominant taxa, including the diatom *Coscinodiscus jonesianus* (49.7%) and *Melosira granulata* (25.0%), chlorophyte *Pediastrum simplex* (4.2%), and the cyanobacterium *Microcystis* sp. (2.7%), marking the first major departure from the pre-shift *Skeletonema*-dominated state. After 2011, when *S. costatum* rebounded to 72.1%, its dominance declined progressively, falling to 50.6% in 2012 and remaining low thereafter despite occasional fluctuations. Concurrently, multiple *Chaetoceros* species, *Pseudonitzschia pungens*, and *Thalassiosira* sp. co-occurred as dominant taxa, indicating increased diatom species richness and functional diversity. Notably, the dinoflagellates *Ceratium fusus* (33.9% in 2014) and *Prorocentrum donghaiense* (4.0% in 2023) appeared among the dominant taxa, suggesting a trend toward greater dinoflagellate representation in the post-shift community (Fig. 5a).

Zooplankton underwent a fundamental shift from small copepod dominance to a mixed assemblage of larger copepods, cladocerans, and gelatinous forms (Fig. 5b). Before 2009, the community was dominated by small size copepods including *Paracalanus parvus* (10.9 to 19.5%), *Acartia bifilosa* (15.4%), *P. crassirostris* (8.2%), and *A. clausi* (6.0%). In 2010, immediately after the shift, *A. pacifica* surged to 62.5% and *Labidocera euchaeta* reached 26.4%, while *Paracalanus* species diclined and the hydrozoan *Blackfordia virginica* appeared as dominant species. During 2011–2012, *Centropages dorsispinatus* became the primary species (14.1% and 29.2%, respectively), accompanied by the cladoceran *Evadne tergestina*,

the larvacean *Oikopleura dioica*, and the chaetognath *Sagitta enflata*. In 2017, the cladoceran *Daphnia* sp. dominated at 71.1%, while *Acartia* spp reached 51.9% in 2021 and *Noctiluca scintillans* dominated in 2022–2023 (50.8% and 64.6%, respectively). This post-shift assemblage represented a transition from small filter-feeding copepods to larger raptorial forms, cladocerans, larvaceans, and chaetognaths, indicating a major shift in trophic structure and energy transfer pathways (Fig. 5b).

Nekton data revealed a directional shift from large fish juveniles to small-sized, lower trophic level taxa. In 2006, the community was dominated by juveniles of large fish species including *Trichiurus haumela* (21.4%), *Lepidotrigla alata* (7.7%), and *Pseudosciaena polyactis* (7.2%). By 2007, the dominant composition shifted to small shrimps (*Exopalaemon carinicauda* and *Palaemon gravieri*, each 14.8%) and the small fish *Coilia mystus* (15.1%). This shift toward smaller size and lower trophic taxa persisted in later years, as observed in 2017 when *Engraulis japonicus* (55.6%) and *Pseudosciaena polyactis* (30.1%) dominated, and in 2023 when *Exopalaemon annandalei* (18.9%) and *Isopoda* sp. (18.5%) were among the top species (Fig. 5c).

Benthos showed a substantial turnover from bivalve-dominated to polychaete- and shrimp-dominated assemblages. In 2010, the bivalve *Corbicula fluminea* accounted for 40.0% of abundance and co-dominated with polychaetes including *Heteromastus filiformis* (20.0%) and *Nephtys* species (20.0%). During 2011–2012, polychaetes including *Heteromastus filiformis* (7.3% and 6.5%), *Lumbrineris* sp. (5.7% and 6.5%), and *Cossurella dimorpha* (4.0% and 10.5%) became dominant while *C. fluminea* declined, and the shrimp *Acetes chinensis* entered the top-five species (5.2% in 2012), reflecting a shift toward more opportunistic, pollution-tolerant taxa (Fig. 5d).

Collectively, these changes demonstrated a consistent pattern of community reorganization across all trophic levels associated with the 2009–2010 regime shift. Before the shift, each group was characterized by a single or few dominant species: phytoplankton by *S. costatum*, zooplankton by small *Paracalanus* and *Acartia copepods*, nekton by large fish juveniles, and benthos by the bivalve *C. fluminea*. After the shift, all groups transitioned toward more diversified and functionally distinct assemblages. Phytoplankton developed greater diatom species richness with increasing dinoflagellate presence; zooplankton shifted to larger

raptorial copepods, cladocerans, and gelatinous forms; nekton moved toward smaller, lower trophic level taxa; and benthos transitioned to polychaete- and shrimp-dominated communities (Fig. 5). These transformations collectively indicated a substantive reorganization of ecosystem structure and function across all trophic levels, consistent with the marked change in community state represented by the multi-taxa PC1 trajectory (Fig. 4).

6 Threshold Analysis of Environmental Factors Driving Ecosystem Regime Shift

To identify environmental thresholds associated with the 2009 regime shift, we examined the response of PC1 to eight environmental variables using a non-parametric derivative method as the primary approach, with GAM-based permutation tests and the exploratory SiZer method used for cross-validation. Among the eight variables, DO, DIN, phosphate, and N/P ratio exhibited significant threshold effects within the historical observation range according to the derivative method with $p < 0.05$; Figs. 6a–d), whereas SST, salinity, Chl a, and pH did not show significant thresholds using any of the three methods (Figs. S5a-d).

Derivative-based analysis identified a significant DO threshold of 6.309 mg/L with a derivative of -3.393 and a 95% confidence interval (CI) from -4.630 to -0.131 ($p<0.05$) (Figs. 6a & S6a). GAM permutation yielded the identical threshold with $p = 0$ (Figs. S7a). SiZer detected a slightly higher value of 6.794 mg/L (Fig. S8a), but we consider the derivative-GAM consensus results more robust. The negative derivative at the threshold indicates that PC1 declines as DO increases beyond the threshold along the response curve. Historical DO concentrations remained above the threshold throughout 2004–2008, ranging from 7.30 to 7.67 mg/L, then began a rapid decline from 7.30 mg/L in 2008 to 7.09 mg/L in 2009, followed by a further drop to 6.50 mg/L in 2010, approaching the threshold and coinciding precisely with the PC1 jump (Fig. 2b). This temporal synchrony between the DO decrease and the PC1 jump, rather than the threshold itself being crossed, underscores the ecological importance of the declining trend and the approach towards a critical level. The persistent high DO levels maintained the system's well-oxygenated baseline, while its sharp decline towards the threshold deteriorating oxygen condition that, through the negative slope of the response curve, drove the ecosystem towards a new community state through the 2009 regime shift.

Derivative-based analysis identified a significant DIN threshold of 1.57 mg/L with a derivative of -0.243 and a 95% CI from -1.015 to -0.069 ($p < 0.05$), indicating a negative slope (Figs. 6b & S6b). GAM permutation yielded the same threshold but with a non-significant p value of 0.231) (Fig. S7b), and SiZer did not detect any threshold. DIN remained mostly above the threshold from 2004 to 2009, ranging from 1.51 to 3.14 mg/L, with values exceeding 2.0 mg/L in most years. DIN fell most abruptly from 2008 to 2009, dropping from 2.18 to 1.65 mg/L, the largest single-year decline in the entire time series, and then further declined to 1.48 mg/L in 2010, crossing below the threshold (Fig. 2f). The rapid downward movement towards and across the threshold, rather than the mere fact of being above it, was the critical feature associated with the regime shift.

A significant phosphate threshold of 0.0381 mg/L was identified via the derivative method with a derivative of 46.27 and a 95% CI from 12.12 to 116.87 ($p < 0.05$), with a positive slope which implies that an increasing phosphate trend could drive PC1 upward (Figs. 6c & S6c). generalized additive model (GAM) permutation yielded a nearly identical threshold of 0.0383 mg/L ($p = 0.010$), while SiZer detected a lower value of 0.0228 mg/L (Figs. S7c & S8b). Phosphate remained below the threshold throughout the study period, yet increased from 0.015 mg/L in 2008 to 0.0205 mg/L in 2009 and then jumped sharply to 0.0379 mg/L in 2010, approaching the threshold with the steepest rise in the entire record. This rapid upward movement towards the threshold was the key process driving the ecosystem response.

For the N/P ratio, the derivative method detected a significant threshold of 23.14 with a derivative of -0.0065 and a 95% CI from -0.0229 to -0.0014 ($p < 0.05$) (Figs. 6d & S6d). GAM permutation yielded the same threshold with a significant p-value of 0.045, while SiZer detected a much higher value of 113.30 (Figs. S7d & S8c). N/P remained far above the threshold from 2004 to 2009, yet declined most sharply from 144 in 2008 to 80 in 2009, the largest single-year reduction in the entire time series, before falling further to 39 in 2010, approaching the threshold. The rapid downward trajectory towards the threshold, rather than the threshold itself being crossed, was the critical driver of the regime shift.

All three methods consistently yielded non-significant results for SST, salinity, Chla, or pH, with p-values exceeding 0.05 for both the derivative method and GAM permutation tests, and SiZer failing to identify any significant derivative regions (Fig. S5). The consistency of

non-significant results across all three methods indicated that these environmental factors did not exhibit detectable threshold effects within their historical ranges of variation.

Integrating the threshold analysis, historical trajectories, and abrupt change of PC1 during the regime shift, four significant environmental factors, namely DO, DIN, phosphate, and N/P ratio exhibited coordinated changes during the 2009 transition (Fig. 6a–d). All four factors exhibited accelerated changes during the 2008–2009 period immediately preceding the shift, and these directional trends continued into 2009–2010, coinciding precisely with the PC1 jump. For DO and phosphate, the changes were even more pronounced in the latter year, while DIN and N/P ratio showed the sharpest declines in the preceding year. Despite these differences in timing, the convergence of these directional changes within the two-year window from 2008 to 2010, rather than the action of any single factor, was the key feature associated with the regime shift. The nutrient-related factors including DIN, phosphate, and N/P ratio all shifted towards alleviation of their respective extreme states, namely DIN surplus, phosphate deficiency, and N/P imbalance, whereas DO moved towards lower oxygen levels and increased hypoxia risk. Despite this fundamental difference in ecological context, all four factors changed simultaneously during 2009–2010 and, and each contributed mathematically to the observed abrupt PC1 rise during the regime shift period through the response-curve relationships between PC1 and the respective environmental drivers.

Discussion

Community Reorganization as Evidence of a Regime Shift

The Yangtze Estuary represents a typical estuarine ecosystem heavily influenced by anthropogenic activities[22], and its high dynamism and complex land-sea interactions confer unique value for revealing the mechanisms of regime shifts in coastal ecosystems[28,33]. Based on a 20-year biological and physio-chemical datasets, our results revealed a coherent ecological story that unfolds across temporal and organizational scales.

At the community level, compositional reorganization manifested as shifts in dominant species and their relative abundances, which preceded any detectable change in α-diversity (Figs. 1a–b)[34]. Phytoplankton diversity reached its lowest value in 2009, while species richness fell by 54% from 2008 to 2009. Zooplankton diversity and richness peaked in 2008 and dropped sharply in 2010. Although species richness began a gradual recovery after 2010, diversity indices remained low, which is consistent with observations from other aquatic systems where rare species proliferate[35]. This decoupling between richness recovery and diversity stagnation indicates that the post-shift community, despite being numerically comparable in species count, had not regained its structural integrity prior to the regime shift[36].

Examination of dominant species turnover across all four biotic groups further corroborated the ecological reality of the 2009 to 2010 regime shift period (Figs. 5a–d). Dominant phytoplankton shifted from near monopoly of a single diatom species to a diversified diatom assemblage with increased species richness (Fig. 5a)[37]. Zooplankton transitioned from small filter-feeding copepods to a mixed assemblage of large raptorial copepods, cladocerans, larvaceans, and chaetognaths, reflecting a major reconstruction of trophic structure and energy transfer pathways (Fig. 5b). Nekton shifted from large fish juveniles to small shrimps and the small fish (Fig. 5c), while benthos changed from bivalve-dominated to polychaete and shrimp dominated community (Fig. 5d)[38,39]. These concurrent turnovers across all four trophic levels, despite their differing ecological functions and life histories, point to a common driver operating at the ecosystem scale rather than group-specific responses.

This compositional signal was captured by the first principal component (PC1) of the multi-taxon community matrix, which exhibited a distinct breakpoint around 2009, corroborated by three independent change-point algorithms and further validated by UPGMA clustering (Figs. 4 & S5b). PC1 values were consistently negative prior to the shift, and then became highly variable with pronounced positive excursions after 2010, indicating a fundamental reorganization of the estuarine ecosystem from one persistent community state to another[40]. Critically, the PC1 breakpoint coincided with concurrent changes in independent biological indicators, including the collapse of phytoplankton diversity, reduction in species richness, and comprehensive dominant species turnover across all four taxonomic groups (Figs. 1 & 5)[41,42]. The sharpest biological response occurred precisely when PC1 crossed from negative to positive values, demonstrating that the multivariate community state captured by PC1 was not merely a statistical abstraction but a faithful reflection of real ecological change.

The convergence of multiple independent lines of evidence firmly establishes the 2009–2010 interval as an ecologically meaningful regime shift, rather than a mere statistical breakpoint[43,44]. The multiple cluster changes after 2009 indicate that the system did not settle into a single stable state but entered a dynamic regime of recurrent compositional adjustments, with cluster shifts observed in 2010–2011, 2018–2019, and 2020–2021 (Fig. S3b). This pattern aligns with the recognition that regime shifts often lead to alternative dynamic regimes marked by recurrent fluctuations, with the post-shift state potentially reinforced by hysteresis even when environmental conditions revert[11]. This pattern aligns with the recognition that regime shifts often lead to alternative dynamic regimes marked by recurrent fluctuations, with the post-shift state potentially reinforced by hysteresis even when environmental conditions revert. The persistence of post-shift community configurations, despite the partial return of some environmental variables towards pre-shift conditions, supports the hysteresis hypothesis and underscores the importance of considering both the magnitude and the direction of ecological change when assessing ecosystem stability[7,45].

Environmental Drivers and Ecological Thresholds of the Regime Shift

dbRDA revealed that at the decades scale, dissolved oxygen (DO) was the only statistically significant driver, explain 22.8% of total community variation (Fig. 3a). The predominance of DO is consistent with the well-documented long-term oxygen depletion in the Yangtze

Estuary, where DO in the nearshore low-DO core descending at a rate of -0.07 mg/(L·a) from 1997 to 2014[32], and the hypoxia intensity has increased over the last half century primarily due to anthropogenic eutrophication[22]. However, year-specific dbRDA analyses revealed pronounced temporal heterogeneity: during the pre-shift period (2004–2009), significant drivers varied across years, typically involving combinations of DO, SST, salinity, and N/P ratio (Fig. 3b). Notably, N/P ratio emerged as a significant driver in 2006, 2007, and again in 2009, when it was the only significant driver. DO also appeared as a significant driver in 2006, while DIN and phosphate did not become significant until the post-shift period. This pattern suggests that the factors driving community variation changed substantially over time. This temporal heterogeneity underscores that no single variable acted as a persistent, exclusive driver of community change throughout the study period[9]. Instead, the ecosystem responded to a shifting suite of environmental stressors, with the relative importance of individual factors changing over time.

Threshold analyses using the non-parametric smooth derivative method captured exactly this multi-driver mechanism (Figs. 6 & S6). GAM-based permutation tests and the exploratory SiZer method were used for cross-validation, with GAM permutation confirming the DO threshold and yielding consistent estimates for the other three factors (Fig. S7 & S8). The negative derivatives for DO, DIN, and N/P ratio indicated that PC1 declined as these variables increased along the response curves, while the positive derivative for phosphate indicated the opposite (Figs. 6a–d). Critically, the trajectories of all four factors during 2007–2010 moved in concert towards or across these boundaries. This synchronized movement, through the response-curve relationships between PC1 and each environmental driver, mathematically contributed to the observed positive PC1 change during 2009–2010 (Fig. 3). Thus, while dbRDA identified DO as the most influential factor over the entire time series, the threshold analyses revealed that the transition was triggered by the synchronized approach of multiple drivers to their respective critical levels, a pattern that would have been obscured if only decadal-scale average relationships were examined[46,47]. The consistency between the multi-driver signal from the year-specific dbRDA results and the concurrent threshold crossings across multiple factors reinforces the interpretation that the 2009 regime shift was a

product of synergistic environmental forcing, rather than the consequence of any single factor exceeding its critical value[48,49].

The identified thresholds and their historical trajectories are strongly supported by independent evidence from the Yangtze Estuary ecosystem. The DO threshold of 6.309 mg/L and its declining trend during 2005–2010 was consistent with the long-term oxygen depletion documented in the region. Liu et al. reported that from 1997 to 2014 the nearshore low DO core descended at -0.07 mg/(L·a), with hypoxia intensifying over the last half century primarily due to anthropogenic eutrophication[32,50]. Our dataset confirmed a sharp decline from 7.67 mg/L in 2007 to 6.50 mg/L in 2010, consistence with the documented extremely low DO years of 2010 related to El Niño signals[32]. Under the negative slope of the PC1–DO response curve, the declining DO trend yields a positive change in PC1 (Fig. S6a). This indicates that the 6.309 mg/L level is an ecological tipping point above which the downward trend in DO, rather than the absolute low concentration, drives the ecosystem state change. Importantly, this threshold is higher than classic definition of hypoxia (<2.0 mg/L). Our threshold marks the concentration around which a decreasing DO trend triggers a community shift, highlighting that the rate and direction of DO change, not merely the crossing of a low oxygen boundary, are critical for structuring the estuarine community. This finding is supported by multiple lines of evidences. Different taxonomic groups exhibit widely varying hypoxia thresholds, and many organisms show behavioral and physiological responses at DO concentrations well above 2 mg/L[51,52]. Spietz et al. demonstrated that bacterial community structure in a seasonally hypoxic estuary shifted at DO concentrations of 5.18–7.12 mg/L[53]. Zooplankton assembly shifted from stochastic to deterministic at approximately 8 mg/L DO, with declining oxygen reducing plankton diversity and weakening cross-trophic interactions[54]. These studies confirm that our threshold represents an ecological early warning level, a concentration around which the rate of DO decline begin to restructure communities long before the system crosses the traditional hypoxia boundary.

The Yangtze Estuary has long been characterized by nitrogen over surplus and chronic phosphorus limitation, resulting in persistently elevated N/P ratios[23,55,56]. From the 1960s to 2000, the annual average DIN concentration increased sharply, while both DIN and phosphate concentrations showed increasing trends from 1984 to 2006, with N/P ratios exhibiting a

decreasing trend over the same period[57-60]. However, this trajectory reversed after around 2005, when DIN concentrations began to decrease, whereas phosphate showed a delayed response with a slow downward trend[58]. More recent data from 2016 to 2021 further confirmed that DIN concentrations in Yangtze Estuary have continued to fluctuated downward, consistent with our post-shift DIN observation[61]. Analyses of data from 2003 to 2010 have noted phosphate concentration exhibiting increasing trends overall on both annual and seasonal timescales from 2007 to 2010[62,63]. Under the negative slopes of the PC1–DIN and PC1–N/P response curves and the positive slope of the PC1–phosphate response curve, the directional changes of DIN decreasing, phosphate increasing, and N/P decreasing collectively produced a positive change in PC1. This indicates the coordinated alleviation of nitrogen over-enrichment, phosphorus limitation, and elevated N/P ratios, rather than the absolute concentration levels themselves, drove the ecosystem state transition. The thresholds of 1.57 mg/L for DIN, 0.0381 mg/L for phosphate, and 23.14 for N/P ratio thus marked a vulnerability zone, indicating that the ecosystem is poised for state change when moved from chronic nutrient imbalance toward a more balanced regime. The directional movements of DIN and N/P ratio are consistent with the post-2005 reversal documented in the literature, while the short-term phosphate increase during the transition period aligns with the broader pattern of nutrient imbalance alleviation[58,64].

Mechanisms Linking Multiple Environmental Drivers to Community Reorganization

The alleviation of nutrient imbalance has consistently triggered non-linear restructuring of biological communities in estuarine ecosystems worldwide. A study based on 30 year concurrent observations in the Dutch Wadden Sea demonstrated that long term variations in limiting phosphate and silicon were strongly correlated with community structures of phytoplankton, macrozoobenthos, and estuarine birds, indicating that nutrient reduction primarily drives compositional and functional reorganization[65]. Similarly, a comparative study before and after the implementation of nutrient mitigation measures in the Eden Estuary, Scotland, revealed that the macrobenthic community showed overall improvements in both structural and functional metrics, confirming that alleviation of nutrient imbalance drives significant changes in benthic community composition[66]. Researches focused on Chinese coastal waters with long term nutrient imbalance pointed out that the implementation of

nutrient management measures and subsequent improvement in nutrient conditions, including declining DIN and phosphate concentrations and shifting N/P ratios, have driven significant changes in biological communities which responded more sensitively than biomass[23,29].

Our biodiversity data from 2004 to 2023 are fully consistent with these findings (Figs. 1a–b, 5a–d). The sharp decline in diversity and richness across all biotic groups during regime shift precisely coincided with the period when our environmental data show obvious DIN declining, phosphate rising, and N/P ratio dropping (Figs. 2f-h). Neither group recovered to their pre-decline peaks afterwards (Figs. 1a–b). The comprehensive turnover of dominant species across all four biotic groups, as detailed above, further confirmed that the direction of nutrient change drove the community transition across multiple trophic levels (Figs. 5a–d). These findings collectively confirmed that in waters subject to long term nutrient imbalance, the alleviation of nutrient surplus and the restoration of stoichiometric balance, rather than changes in absolute nutrient concentrations alone, have become critical drivers reshaping biological communities[26,67].

In contrast to the nutrient-related factors, the mechanism for DO was fundamentally different but equally consequential. Rather than alleviating stress, DO moved towards lower oxygen levels and increased hypoxia risk (Fig. 2b)[29,32,58,63]. This paradoxical convergence suggests that the ecosystem responded to the cumulative effect of multiple simultaneous changes, rather than to a single trajectory of improvement or degradation[68,69]. The reorganization of trophic structure, including the shift from small filter-feeding copepods to large raptorial copepods and from bivalve-dominated benthos to polychaete- and shrimp-dominated communities, reflects a fundamental shift in energy transfer pathways and ecosystem functioning (Figs. 5b, 5d). This restructuring indicates that the regime shift was not merely a change in species composition but a reconfiguration of energy and material flow through the ecosystem[13]. Critically, the simultaneous occurrence of nutrient alleviation and oxygen depletion during 2009–2010, rather than their individual effects, created a synergistic forcing that pushed the ecosystem across the tipping point (Figs. 2b, 2f–h, 4, 5). This multi-driver synergy, in which opposing environmental changes converged to produce a single ecological outcome, underscores the importance of considering multiple interacting

stressors rather than single-factor explanations in understanding ecosystem regime shifts in coastal environments[49,70,71].

Implications for Ecosystem Management

The temporal convergence of all four factors, despite their differing ecological roles, created a synergistic forcing that pushed the ecosystem across a critical transition. This pattern aligns with a growing body of evidence of regime shifts typically arised from multiple drivers acting in concert rather than any single factor in isolation[49,72,73]. Individual stressors may be insufficient to induce a state change, yet when multiple factors converge synergistically, they can erode ecosystem resilience and lower the critical thresholds for regime shifts[12,74,75]. The cumulative effects of interacting stressors often produce non-additive responses that would be overlooked if only average relationships or single drivers were examined[76]. This underscores the value of threshold-based diagnostics that integrate multiple interacting drivers to anticipate ecological regime shifts, as demonstrated in recent multi-factor analytical frameworks applied to coastal ecosystems[75,77].

Importantly, this regime shift does not imply movement of ecosystem towards a better or worse state, as PC1 is a statistical composite of species abundance patterns rather than a measure of ecological quality. The transition instead represents a shift from one persistent state to another, driven by the convergence of multiple environmental trends that collectively reorganized the ecosystem structure. After the regime shift, the ecosystem entered a new stable state in which the trigger factors became the new baseline, consistent with the theory of alternative stable states[78]. Under this framework, multiple stable states can coexist under the same environmental conditions, and once a transition occurs, the system may not return to its original state even if environmental conditions revert, a phenomenon known as hysteresis[7,79]. This is precisely what we observed: although the trigger factors remained above their threshold after the shift, the ecosystem did not revert to its pre-shift configuration.

Traditional management approaches that focus on single stressors and attempt to maintain conditions below a single threshold may be inadequate for systems subject to multiple interacting drivers. Our results instead suggest that management strategies should monitor the simultaneous trajectories of multiple environmental factors, particularly their rates of change, rather than focusing solely on absolute concentrations[68,69]. They should also recognize that

alleviation of one stressor may be offset by intensification of another, as observed with DO in our case[80]. Finally, managers must consider that ecosystems may transition to new stable states that are resistant to reversal even when conditions are restored[36]. These insights call for a shift from single-factor management toward integrated, multi-driver approaches that account for the complex interactions and temporal dynamics inherent in coastal ecosystems[69,81].

Methods

1. Biological and Physiochemical Dataset

Biological data used in this study were obtained from the National Marine Data and Information Service (NMDIS), China, comprising field survey records in the Yangtze Estuary from 2004 to 2023 across four biotic compartments: phytoplankton, zooplankton, nekton, and benthos (Fig. S9a). Duplicate entries were merged and invalid records were removed to generate a standardized analytical dataset. Given that summer sampling yielded the most comprehensive and temporally consistent coverage over the study period, while the remaining seasons are characterized by considerable data deficiencies, we consequently restrict our investigation to the summer months. For each biotic group, species richness and the Shannon diversity index were calculated to characterize inter-annual variations in community structure[34]. Meanwhile, dominant species of each group were identified annually by ranking the relative percentage of each species' summer abundance relative to the total annual abundance, selecting the top five species each year, and their temporal trajectories were plotted to track changes in dominance over time[82].

Physico-chemical variables data were assembled from three complementary sources to ensure spatiotemporal continuity. The primary in-situ measurements were sourced from the National Marine Data and Information Service (NMDIS), conducted concurrent with the biological surveys. This observational baseline was complemented by satellite-derived reanalysis products from the Copernicus Marine Service (CMEMS), specifically the sea surface temperature product 010-011 and biogeochemical product 001-029[83,84]. Additionally spatial coverage was provided by the monthly gridded water quality dataset of Lin et al., which was derived from in-situ measurements conducted by the National Marine Environmental Monitoring Center (NMEMC)[85]. Gridded environmental data from CMEMS were extracted using Python following the protocols described in the Copernicus Marine Help Center[86], while the Lin dataset was processed with ArcGIS Pro (V3.5.0)[87]. All environmental data were assigned to biological stations by nearest-neighbor extraction and then combined with the in-situ measurements to form a unified dataset for subsequent analyses (Fig. S9b).

Stations with the same sampling time and coordinates (to four decimal places) were considered identical across all data integration steps, including biological environmental matching and multi-source spatial matching.

2. Distance-Based Redundancy Analysis (dbRDA)

To assess the overall influence of environmental factors on the inter-annual variability of community composition across the four biotic groups, we performed distance-based redundancy analysis (dbRDA) using the capscale function in the vegan R package (V2.7.3)[17,88,89]. The community composition matrix was transformed using Hellinger distance to reduce the weight of rare species. Environmental variables were standardized to zero mean and unit variance prior to analysis. A global model including all seven environmental variables (SST, salinity, DO, pH, Chl a, DIN, and phosphate) was fitted, and the significance of each variable was tested using 999 permutations. In addition to the decade scale analysis, year-specific dbRDA was conducted for each year with sufficient biological data to examine temporal heterogeneity in the identity and number of significant environmental drivers. This year-specific approach allowed us to detect whether the dominant drivers of community composition shifted over time, particularly before versus after the regime shift[46,90].

3. Identification of Ecosystem Regime Shift based on PCA analysis

To identify potential regime shifts in the ecosystem, principal component analysis (PCA) was performed on the species abundance data of all four biotic groups combined. The first principal component (PC1), which explained 41.57% of the total variance, was used as an integrative indicator of ecosystem state. To avoid false positives from any single method, three independent techniques were applied to the PC1 time series for breakpoint detection: the PELT (Pruned Exact Linear Time) algorithm with a BIC penalty and a minimum segment length of 2, as implemented in the changepoint R package (V2.3)[91]; the Bai-Perron structural change test, performed via the breakpoints function in the strucchange R package (V1.5.4)[92]; and a sliding-window procedure with a window size of four years, which combined Wilcoxon rank-sum tests ($\alpha = 0.1$) with bootstrap resampling (199 iterations) of mean differences to evaluate the statistical significance of potential shifts[93]. A consensus breakpoint year was identified only when at least two methods agreed on the same year. To further validate

ecological continuity, we performed UPGMA hierarchical clustering based on Bray-Curtis dissimilarity of community composition, using the vegdist and hclust functions from the vegan R package[94]. A regime-shift year was confirmed when a PCA-derived breakpoint fell within one year of a clustering-detected change. In addition, PCA was repeated separately for each biotic group to compare the breakpoints obtained from individual groups versus the integrated dataset, thereby demonstrating the necessity of a multi-group approach.

4. Environmental Variables Thresholds Associated with Ecosystem Regime Shift

To identify the ecological thresholds of environmental drivers beyond which the ecosystem state (PC1) is likely to undergo a regime shift, we adopted the non-parametric smooth derivative method as our primary analytic tool[95-97]. This approach computes the first derivative of the fitted response curve, identifies the point of maximum absolute derivative as a candidate threshold, and rigorously tests its statistical significance via bootstrap-based confidence intervals, thereby providing an objective and statistically defensible criterion for distinguishing true threshold effects from random fluctuations along the gradient[73]. The derivative method was implemented using mgcv R package (V1.9.4) for GAM fitting, while derivative calculations and moving average smoothing were performed with zoo R package (V1.8.15)[97,98].

For cross validation, both GAM-based permutation test and the exploratory Significant Zero Crossings method (SiZer) were applied. GAM-based permutation tests evaluated threshold credibility by comparing observed deviance to a null distribution generated from 199 permutations of the environmental variable, with thresholds considered significant when the p-value fell below 0.05, also using mgcv package[99,100]. SiZer employs locally weighted polynomial regression across a range of bandwidth values to examine how the first derivative of the response function changes along the environmental gradient[19,101]. Unlike the derivative method, SiZer offers a graphical representation of derivative significance across multiple smoothing scales rather than providing a single threshold estimate with p-value or confidence interval. Given the subjective bandwidth selection and the risk of over- or under-smoothing[21], we treated SiZer strictly as an exploratory corroboration tool, implemented via SiZer R package (V0.1.8)[19].

Reference

1 Seitz, R. D., Wennhage, H., Bergström, U., Lipcius, R. N. & Ysebaert, T. Ecological value of coastal habitats for commercially and ecologically important species. *ICES J. Mar. Sci.* **71**, 648-665 (2014).

2 Barbier, E. B. *et al.* The value of estuarine and coastal ecosystem services. *Ecol. Monogr.* **81**, 169-193 (2011).

3 Ward, N. D. *et al.* Representing the function and sensitivity of coastal interfaces in Earth system models. *Nat. Commun.* **11**, 2458; 10.1038/s41467-020-16236-2 (2020).

4 He, Q. & Silliman, B. R. Climate change, human impacts, and coastal ecosystems in the Anthropocene. *Curr. Biol.* **29**, R1021-R1035; 10.1016/j.cub.2019.08.042 (2019).

5 Li, C. & Fang, S. Coastal Land Use Transitions and Their Cascading Impacts on Ecosystem Resilience: A Global Bibliometric Review. *Reg. Eco. Manag.* **1**, 7; 10.53941/rem.2026.100007 (2026).

6 Lotze, H. K. *et al.* Depletion, degradation, and recovery potential of estuaries and coastal seas. *Science* **312**, 1806-1809 (2006).

7 Scheffer, M. & Carpenter, S. R. Catastrophic regime shifts in ecosystems: linking theory to observation. *Trends Ecol. Evol.* **18**, 648-656 (2003).

8 Andersen, T., Carstensen, J., Hernández-García, E. & Duarte, C. M. Ecological thresholds and regime shifts: approaches to identification. *Trends Ecol. Evol.* **24**, 49-57 (2009).

9 Djeghri, N., Boyé, A., Ostle, C. & Hélaouët, P. Reinterpreting two regime shifts in North Sea plankton communities through the lens of functional traits. *Global Ecol. Biogeogr.* **32**, 962-975 (2023).

10 Kortsch, S. *et al.* Disentangling temporal food web dynamics facilitates understanding of ecosystem functioning. *J. Anim. Ecol.* **90**, 1205-1216 (2021).

11 Möllmann, C., Folke, C., Edwards, M. & Conversi, A. Marine regime shifts around the globe: theory, drivers and impacts. *Philos. T. R. Soc. B* **370**, 20130260; 10.1098/rstb.2013.0260 (2015).

12 Sguotti, C., Vasilakopoulos, P., Tzanatos, E. & Frelat, R. Resilience assessment in complex natural systems. *P. Roy. Soc. B-Biol. Sci.* **291**, 20240089; 10.1098/rspb.2024.0089 (2024).

13 deYoung, B. *et al.* Regime shifts in marine ecosystems: detection, prediction and management. *Trends Ecol. Evol.* **23**, 402-409 (2008).

14 Litzow, M. A. & Mueter, F. J. Assessing the ecological importance of climate regime shifts: An approach from the North Pacific Ocean. *Prog. Oceanogr.* **120**, 110-119 (2014).

15 Morse, R., Friedland, K., Tommasi, D., Stock, C. & Nye, J. Distinct zooplankton regime shift patterns across ecoregions of the US Northeast continental shelf Large Marine Ecosystem. *J. Marine Syst.* **165**, 77-91 (2017).

16 González Sagrario, M. d. l. Á., Vrede, T. & Belle, S. Late Holocene cooling drove drastic decreases in cladoceran diversity in a subarctic lake. *Sci. Rep-UK* **14**, 30490; 10.1038/s41598-024-81690-7 (2024).

17 Legendre, P. & Anderson, M. J. Distance-based redundancy analysis: testing multispecies responses in multifactorial ecological experiments. *Ecol. Monogr.* **69**, 1-24 (1999).

18 Detmer, A. R. *et al.* Evaluating the robustness of generalized additive models as a tool for threshold detection in variable environments. *Ecosphere* **16**, e70117; 10.1002/ecs2.70117 (2025).

19 Sonderegger, D. L., Wang, H., Clements, W. H. & Noon, B. R. Using SiZer to detect thresholds in ecological data. *Front. Ecol. Evol.* **7**, 190-195 (2009).

20 Large, S. I., Fay, G., Friedland, K. D. & Link, J. S. Defining trends and thresholds in responses of ecological indicators to fishing and environmental pressures. *ICES J. Mar. Sci.* **70**, 755-767 (2013).

21 D'Amario, S. C. *et al.* The prevalence of nonlinearity and detection of ecological breakpoints across a land use gradient in streams. *Sci. Rep-UK.* **9**, 3878; 10.1038/s41598-019-40349-4 (2019).

22 Sheng, H. *et al.* Anthropogenic eutrophication and stratification strength control hypoxia in the Yangtze Estuary. *Commun. Earth Environ.* **5**, 235; 10.1038/s43247-024-01403-w (2024).

23 Shi, S., Xu, Y., Li, W. & Ge, J. Long-term response of an estuarine ecosystem to drastic nutrients changes in the Changjiang River during the last 59 years: A modeling perspective. *Front. Mar. Sci.* **9**, 1012127; 10.3389/fmars.2022.1012127 (2022).

24 Zhou, Z. *et al.* Dam-driven phosphorus sinks reversed the anticipated increase in phosphorus export from the Yangtze River Basin. *Commun. Earth Environ.* **7**, 69; 10.1038/s43247-025-03087-2 (2025).

25 Xue, W. *et al.* Comparative study on sea-level rise in the Yangtze River Estuary and Red River Estuary in the recent 30 years. *Sci. Rep-UK* **15**, 35938; 10.1038/s41598-025-02232-3 (2025).

26 Wang, Y., Xu, H. & Li, M. Long-term changes in phytoplankton communities in China's Yangtze Estuary driven by altered riverine fluxes and rising sea surface temperature. *Geomorphology* **376**, 107566; 10.1016/j.geomorph.2020.107566 (2021).

27 Chen, K. *et al.* Nutrient regimes shaping the diatom-dinoflagellate interdecadal succession in coastal temperate waters of China. *Water Res.*, 125278; 10.1016/j.watres.2025.125278 (2025).

28 Lin, J. *et al.* Regime shifts in the Changjiang (Yangtze River) Estuary: The role of concentrated benthic suspensions. *Mar. Geol.* **433**, 106403 (2021).

29 Peng, J. *et al.* Threshold responses of plankton community structure to nutrient gradients and environmental drivers in the Yangtze River estuary. *Mar. Pollut. Bull.* **223**, 118881; 10.1016/j.marpolbul.2025.118881 (2026).

30 Fan, J., Li, J., Xie, Y., Zhang, H. & Jiang, X. Synchronous responses to tidal restriction by seawall construction across fish and plankton communities in Yangtze River Estuary. *Mar. Environ. Res.* **210**, 107312; 10.1016/j.marenvres.2025.107312 (2025).

31 Gao, X. *et al.* Regime shift in fish assemblage structure in the Yangtze River following construction of the Three Gorges Dam. *Sci. Rep-UK* **9**, 4212; 10.1038/s41598-019-38993-x (2019).

32 Liu, A. *et al.* Inter-annual variations of dissolved oxygen and hypoxia off the northern Changjiang River (Yangtze River) Estuary in summer from 1997 to 2014. *Acta Oceanol. Sin.* **43**, 119-130 (2024).

33 Zhang, D. *et al.* Sediment dynamics in the mudbank of the Yangtze River Estuary under regime shift of source and sink. *Int. J. Sediment Res.* **37**, 97-109 (2022).

34 Magurran, A. E. Measuring biological diversity. *Curr. Biol.* **31**, R1174-R1177; 10.1016/j.cub.2021.07.049 (2021).

35 Dittrich, J., Dias, J. D., de Paula, A. C. M. & Padial, A. A. Experimental nutrient enrichment increases plankton taxonomic and functional richness and promotes species dominance overtime. *Hydrobiologia* **850**, 4029-4048 (2023).

36 Dullaert, E. C. *et al.* Response of the mesozooplankton community in the western Gulf of Maine to changing oceanographic conditions: the 2010 regime shift. *J. Plankton Res.* **48**, fbaf066; 10.1093/plankt/fbaf066 (2026).

37 Wei, Y. *et al.* Summer regime shift in an estuarine ecosystem over decades: Evidence from dominant-taxon downsizing and warm-water species expansion. *Water Res.* **305**, 126467; 10.1016/j.watres.2026.126467 (2026).

38 Yan, J. *et al.* Long-term variation of the macrobenthic community and its relationship with environmental factors in the Yangtze River estuary and its adjacent area. *Mar. Pollut. Bull.* **123**, 339-348 (2017).

39 Eklöf, J. S. *et al.* A spatial regime shift from predator to prey dominance in a large coastal ecosystem. *Commun.Biol.* **3**, 459; 10.1038/s42003-020-01180-0 (2020).

40 Beck, M. *et al.* Morphological diversity increases with decreasing resources along a zooplankton time series. *P. Roy. Soc. B-Biol. Sci.* **290**, 20232109; 10.1098/rspb.2023.2109 (2023).

41 Weijerman, M., Lindeboom, H. & Zuur, A. Regime shifts in marine ecosystems of the North Sea and Wadden Sea. *Mar. Ecol. Prog. Ser.* **298**, 21-39 (2005).

42 Bernal-Ibáñez, A. *et al.* Concomitant effects of algae invasion and sea urchin mass mortality drive the shift from barrens to turf grounds. *Mar. Environ. Res.* **213**, 107646; 10.1016/j.marenvres.2025.107646 (2026).

43 Schlüter, M. H., Merico, A., Wiltshire, K. H., Greve, W. & Von Storch, H. A statistical analysis of climate variability and ecosystem response in the German Bight. *Ocean Dynam.* **58**, 169-186 (2008).

44 Tomczak, M. T. *et al.* Ecological network indicators of ecosystem status and change in the Baltic Sea. *PLoS one* **8**, e75439; 10.1371/journal.pone.0075439 (2013).

45 Occhipinti, G., Valenti, D. & Lazzari, P. Alternative dynamic regimes of plankton communities in perturbed environments. *EGUsphere* **2025**, 1-27; 10.5194/egusphere-2025-2994 (2025).

46 Castillo-Escrivà, A., Mesquita-Joanes, F. & Rueda, J. Effects of the temporal scale of observation on the analysis of aquatic invertebrate metacommunities. *Front. Ecol. Evol.* **8**, 561838; 10.3389/fevo.2020.561838 (2020).

47 Shoemaker, L. G. *et al.* The long and the short of it: Mechanisms of synchronous and compensatory dynamics across temporal scales. *Ecology* **103**, e3650; 10.1002/ecy.3650 (2022).

48 Möllmann, C., Folke, C., Edwards, M. & Conversi, A. Marine regime shifts around the globe: theory, drivers and impacts. *Philosophical Transactions of the Royal Society B: Biological Sciences* **370**, 20130260 (2015).

49 Rocha, J., Yletyinen, J., Biggs, R., Blenckner, T. & Peterson, G. Marine regime shifts: drivers and impacts on ecosystems services. *Philos. T. R. Soc. B* **370**, 20130273; 10.1098/rstb.2013.0273 (2015).

50 Lu, W. *et al.* The temporal-spatial distribution and changes of dissolved oxygen in the Changjiang Estuary and its adjacent waters for the last 50 a. *Acta Oceanol. Sin.* **36**, 90-98 (2017).

51 Vaquer-Sunyer, R. & Duarte, C. M. Thresholds of hypoxia for marine biodiversity. *Proc. Nat. Acad. Sci.* **105**, 15452-15457 (2008).

52 Zhang, W., Han, S., Zhang, D., Shan, B. & Wei, D. Variations in dissolved oxygen and aquatic biological responses in China's coastal seas. *Environ. Res.* **223**, 115418; 10.1016/j.envres.2023.115418 (2023).

53 Spietz, R. L., Williams, C. M., Rocap, G. & Horner-Devine, M. C. A dissolved oxygen threshold for shifts in bacterial community structure in a seasonally hypoxic estuary. *PloS one* **10**, e0135731; 10.1371/journal.pone.0135731 (2015).

54 Zheng, F. *et al.* Associations of oxygen availability with eukaryotic plankton assembly and coalescence in river–lake ecotones. *Ecol. Inform.*, 103787; 10.1016/j.ecoinf.2026.103787 (2026).

55 Li, J., Gao, Y., Bao, Y., Gao, X. & Glibert, P. M. Summer phytoplankton photosynthetic characteristics in the Changjiang River Estuary and the adjacent East China Sea. *Front. Mar. Sci.* **10**, 1111557; 10.3389/fmars.2023.1111557 (2023).

56 Liu, H., Xu, W.-S., Kang, H.-X., Yin, B.-S. & Yang, D.-Z. in *International Conference on Intelligent Computing for Sustainable Energy and Environment.* 188-197 (Springer).

57 Wan, X., Lu, X., Zhu, L. & Feng, J. Relative prevalence of top-down versus bottom-up control in planktonic ecosystem under eutrophication and climate change: A comparative study of typical bay and estuary. *Water Res.* **255**, 121487; 10.1016/j.watres.2024.121487 (2024).

58 Liu, J. *et al.* Change of the long-term nitrogen and phosphorus in the Changjiang (Yangtze) River Estuary. *Front. Mar. Sci.* **9**, 885311; 10.3389/fmars.2022.885311 (2022).

59 Chai, C., Yu, Z., Song, X. & Cao, X. The status and characteristics of eutrophication in the Yangtze River (Changjiang) Estuary and the adjacent East China Sea, China. *Hydrobiologia* **563**, 313-328 (2006).

60 Li, L., Xv, G., Zheng, Y. & Jiang, M. Seasonal characteristics of nutrient and nutrient structure in the Yangtze River estuary. *Arch. Environ. Prot.* **49**, 115-122 (2023).

61 He, B.-z. *et al.* Spatiotemporal characteristics of nutrients in the Yangtze River Estuary from 2016 to 2021 and their influencing factors. *Res. Environ. Sci.*, 221-232 (in Chinese) (2024).

62 Chen, Y. *et al.* Spatial and temporal variations in nitrogen and phosphorous nutrients in the Yangtze River Estuary. *Mar. Pollut. Bull.* **64**, 2083-2089 (2012).

63 Yang, Y. & Xu, R. The environment variation trend in the Changjiang River Estuary in the past 30a. *Mar. Sci.* **39**, 101-107 (in Chinese) (2015).

64 Chen, H., Sun, C. & Wu, Y. Analysis of trend of nutrient structure and infl uencing factors in Changjiang River estuary and its adjacent sea during 23 years. *Mar. Environ. Sci.* **30**, 551-563 (in Chinese) (2011).

65 Philippart, C. J. *et al.* Impacts of nutrient reduction on coastal communities. *Ecosystems* **10**, 95-118 (2007).

66 Watson, S. C., Paterson, D. M., Widdicombe, S. & Beaumont, N. J. Evaluation of estuarine biotic indices to assess macro-benthic structure and functioning following nutrient remediation actions: A case study on the Eden estuary Scotland. *Reg. Stud. Mar. Sci.* **24**, 379-391 (2018).

67 Li, Y. *et al.* Silicon-mediated stoichiometric controls on phytoplankton community shifts in the Yangtze and Yellow Rivers. *J. Hydrol.* **678**, 136031; 10.1016/j.jhydrol.2026.136031 (2026).

68 De Laender, F. Community- and ecosystem-level effects of multiple environmental change drivers: Beyond null model testing. *Global Change Biol.* **24**, 14382; 10.1111/gcb.14382 (2018).

69 Côté, I. M., Darling, E. S. & Brown, C. J. Interactions among ecosystem stressors and their importance in conservation. *P. Roy. Soc. B-Biol. Sci.* **283**, 20152592; 10.1098/rspb.2015.2592 (2016).

70 Bertocci, I. *et al.* Compounded perturbations in coastal areas: contrasting responses to nutrient enrichment and the regime of storm-related disturbance depend on life-history traits. *Funct. Ecolo.* **31**, 1122-1134 (2017).

71 Sguotti, C., Färber, L. & Romagnoni, G. in *Reference Module in Earth Systems and Environmental Sciences* (Elsevier, 2022).

72 Conversi, A. *et al.* A holistic view of marine regime shifts. *Philos. T. R. Soc. B* **370**, 20130279; 10.1098/rstb.2013.0279 (2015).

73 Ratajczak, Z. *et al.* Abrupt change in ecological systems: inference and diagnosis. *Trends Ecol. Evol.* **33**, 513-526 (2018).

74 Polst, B. H. *et al.* Warming lowers critical thresholds for multiple stressor–induced shifts between aquatic primary producers. *Sci. Total Environ.* **838**, 156511; 10.1016/j.scitotenv.2022.156511 (2022).

75 Huang, H. *et al.* Holistic Evolution of the Bohai Sea Complex System: Insights from Interacting Drivers. *Mar. Environ. Res.*, 107905; 10.1016/j.marenvres.2026.107905 (2026).

76 Stockbridge, J., Jones, A. R., Brown, C. J., Doubell, M. J. & Gillanders, B. M. Incorporating stressor interactions into spatially explicit cumulative impact assessments. *Ecol. Appl.* **35**, e3056; 10.1002/eap.3056 (2025).

77 Carrier-Belleau, C., Pascal, L., Nozais, C. & Archambault, P. Tipping points and multiple drivers in changing aquatic ecosystems: A review of experimental studies. *Limnol. Oceanogr.* **67**, S312-S330; 10.1002/lno.11978 (2022).

78 Atela, M. *et al.* Climate-driven regime shift associated with range contraction at warm range edge of Macrocystis pyrifera forests. *Mar. Biol.* **173**, 146; 10.1007/s00227-026-04908-4 (2026).

79 Duarte, C. M., Conley, D. J., Carstensen, J. & Sánchez-Camacho, M. Return to Neverland: shifting baselines affect eutrophication restoration targets. *Estuar. Coast.* **32**, 29-36 (2009).

80 Carrier-Belleau, C., Pascal, L., Tiegs, S. D., Nozais, C. & Archambault, P. Tipping point arises earlier under a multiple-stressor scenario. *Sci. Rep-UK.* **13**, 16780; 10.1038/s41598-023-44012-x (2023).

81 Beauchesne, D., Cazelles, K., Daigle, R. M., Gravel, D. & Archambault, P. Ecological interactions amplify cumulative effects in marine ecosystems. *Sci. Adv.* **11**, eadp9315; 10.1126/sciadv.adp9315 (2025).

82 Blaber, S., Brewer, D. & Salini, J. Species composition and biomasses of fishes in different habitats of a tropical northern Australian estuary: their occurrence in the adjoining sea and estuarine dependence. *Estuar. Coast. Shelf S.* **29**, 509-531 (1989).

83 Perruche, C. Product user manual for the Global Ocean Biogeochemistry Hindcast GLOBAL_REANALYSIS_BIO_001_029, Version 1, Copernicus Marine Environmental Monitoring Service,[data set], 17 pp, (2018).

84 Worsfold, M. *et al.* EU Copernicus Marine Service Quality Information Document for the Global Ocean OSTIA Sea Surface Temperature Reprocessing, SST_GLO_SST_L4_REP_OBSERVATIONS_010_011, issue 1.4, (2022).

85 Lin, J. *et al.* An extensive spatiotemporal water quality dataset covering four decades (1980-2022) in China., (2023).

86 Anais, P. How to open and visualize Copernicus Marine Data using Python?, <https://help.marine.copernicus.eu/en/articles/4854800-how-to-open-and-visualize-copernicus-marine-data-using-python> (2026).

87 Fattorini, L., Marcheselli, M., Pisani, C. & Pratelli, L. Design-based properties of the nearest neighbor spatial interpolator and its bootstrap mean squared error estimator. *Biometrics* **78**, 1454-1463 (2021).

88 Package 'vegan' (2013).

89 Dixon, P. VEGAN, a package of R functions for community ecology. *Journal of vegetation science* **14**, 927-930 (2003).

90 Mäkinen, J. *et al.* The pace and drivers of community change vary over space and time–findings from a national biomonitoring programme. *Ecography* **2025**, e07335; 10.1002/ecog.07335 (2025).

91 changepoint: An R package for changepoint analysis (2014).

92 strucchange: An R package for testing for structural change in linear regression models (2002).

93 Pélissié, M., Devictor, V. & Dakos, V. A systematic approach for detecting abrupt shifts in ecological timeseries. *Biol. Conserv.* **290**, 110429; 10.1016/j.biocon.2023.110429 (2024).

94 Dixon, P. VEGAN, a package of R functions for community ecology. *J. Veg. Sci.* **14**, 927-930 (2003).

95 Simpson, G. L. Modelling palaeoecological time series using generalised additive models. *Front. Ecol. Evol.* **6**, 396134; 10.3389/fevo.2018.00149 (2018).

96 Francesco Ficetola, G. & Denoël, M. Ecological thresholds: an assessment of methods to identify abrupt changes in species–habitat relationships. *Ecography* **32**, 1075-1084 (2009).

97 Wood, S. N. *Generalized additive models: an introduction with R*. (chapman and Hall/CRC, 2017).

98 zoo: S3 Infrastructure for Regular and Irregular Time Series (2005).

99 Ciannelli, L., Chan, K.-S., Bailey, K. M. & Stenseth, N. C. Nonadditive effects of the environment on the survival of a large marine fish population. *Ecology* **85**, 3418-3427 (2004).

100 Young, R. L., Weinberg, J., Vieira, V., Ozonoff, A. & Webster, T. F. Generalized additive models and inflated type I error rates of smoother significance tests. *Comput. Stat. Data An.* **55**, 366-374 (2011).

101 Chaudhuri, P. & Marron, J. S. SiZer for Exploration of Structures in Curves. *J. Am. Stat. Assoc.* **94**, 807-823 (1999).

Figures

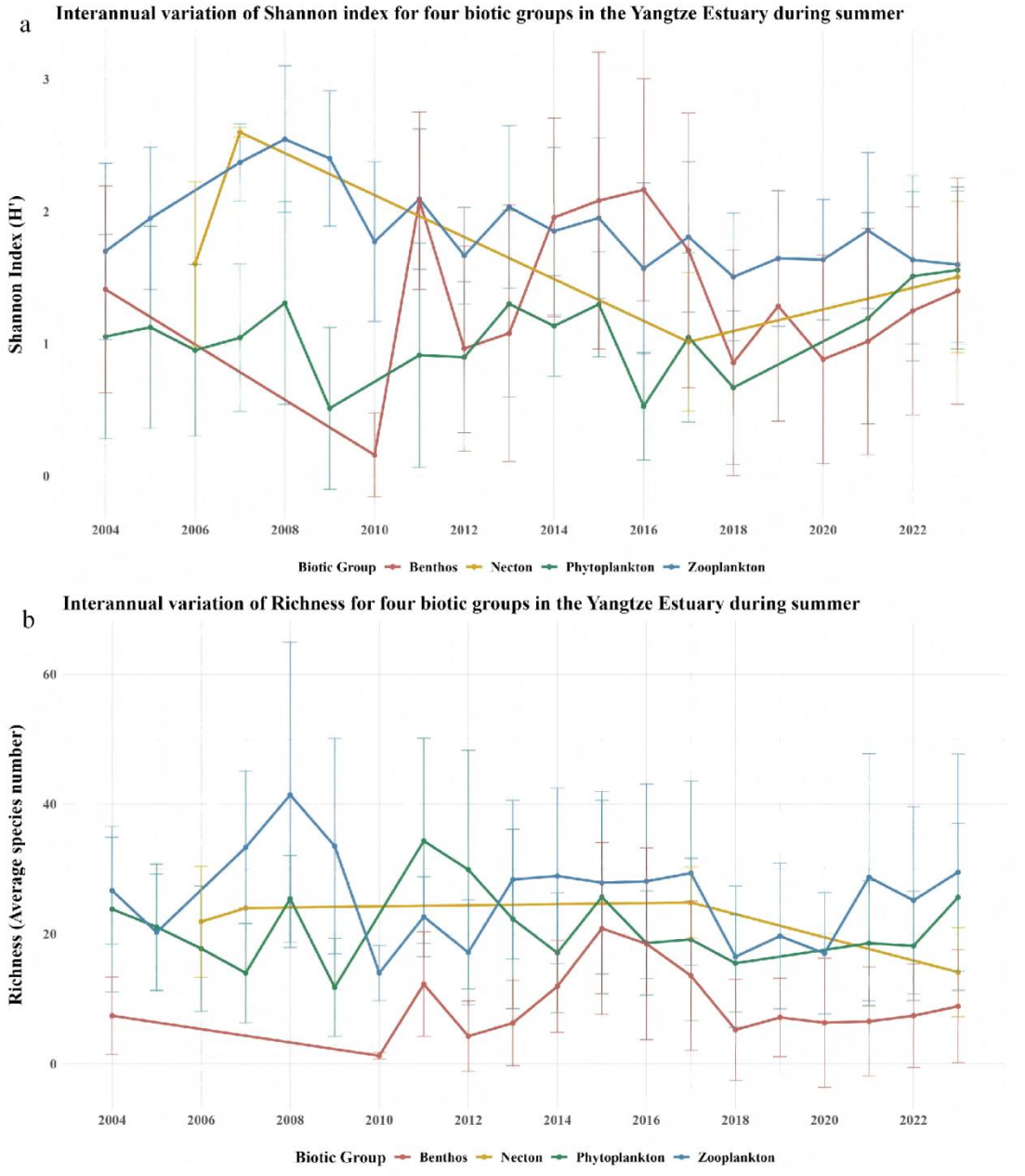


Fig. 1 | Inter-annual variations in summer diversity and species richness for four biotic groups in the Yangtze Estuary from 2004 to 2023.

a Shannon diversity index for phytoplankton, zooplankton, nekton, and benthos. **b** Species richness for phytoplankton, zooplankton, nekton, and benthos.

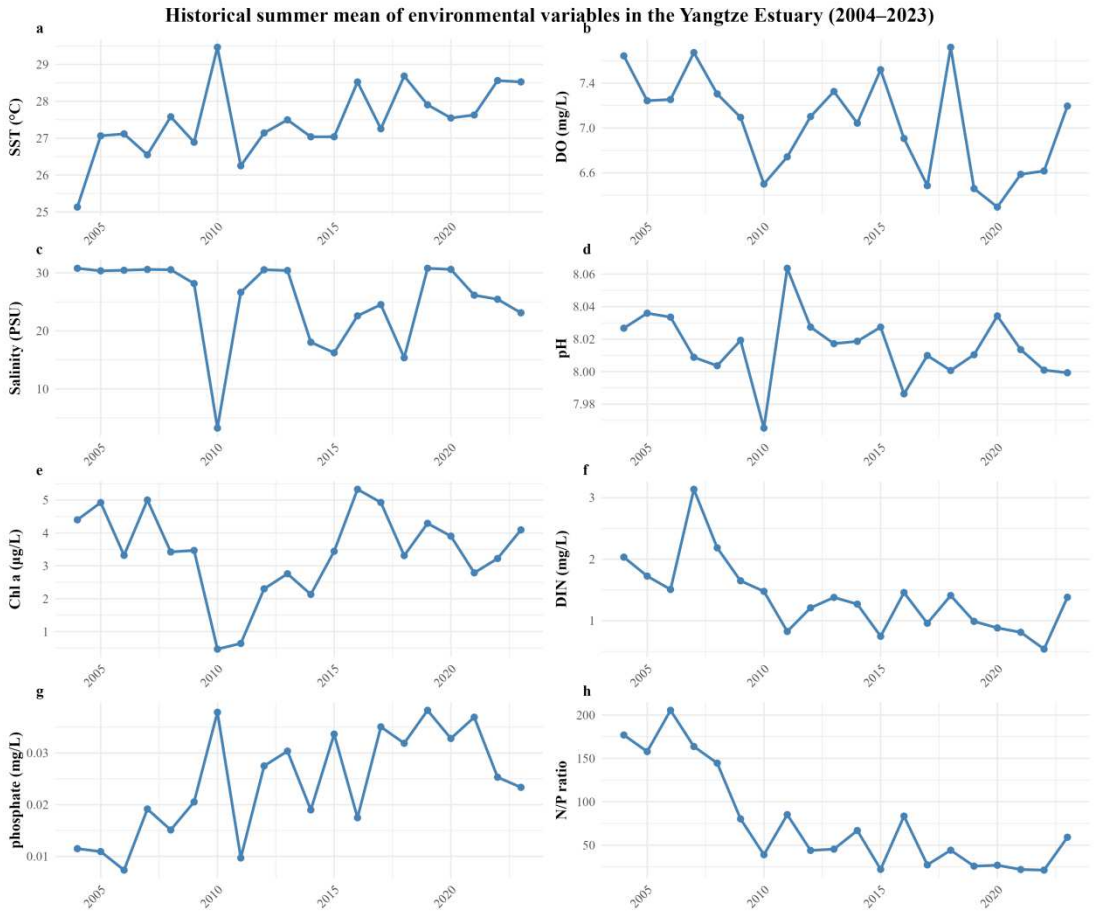


Fig. 2 | Inter-annual change of summer means of eight environmental variabless in the Yangtze Estuary from 2004 to 2023.

a Sea surface temperature (SST). **b** Dissolved oxygen (DO). **c** Salinity. **d** pH. **e** Chlorophyll *a* (Chl *a*). **f** Dissolved inorganic nitrogen (DIN). **g** Phosphate. **h** N/P ratio.

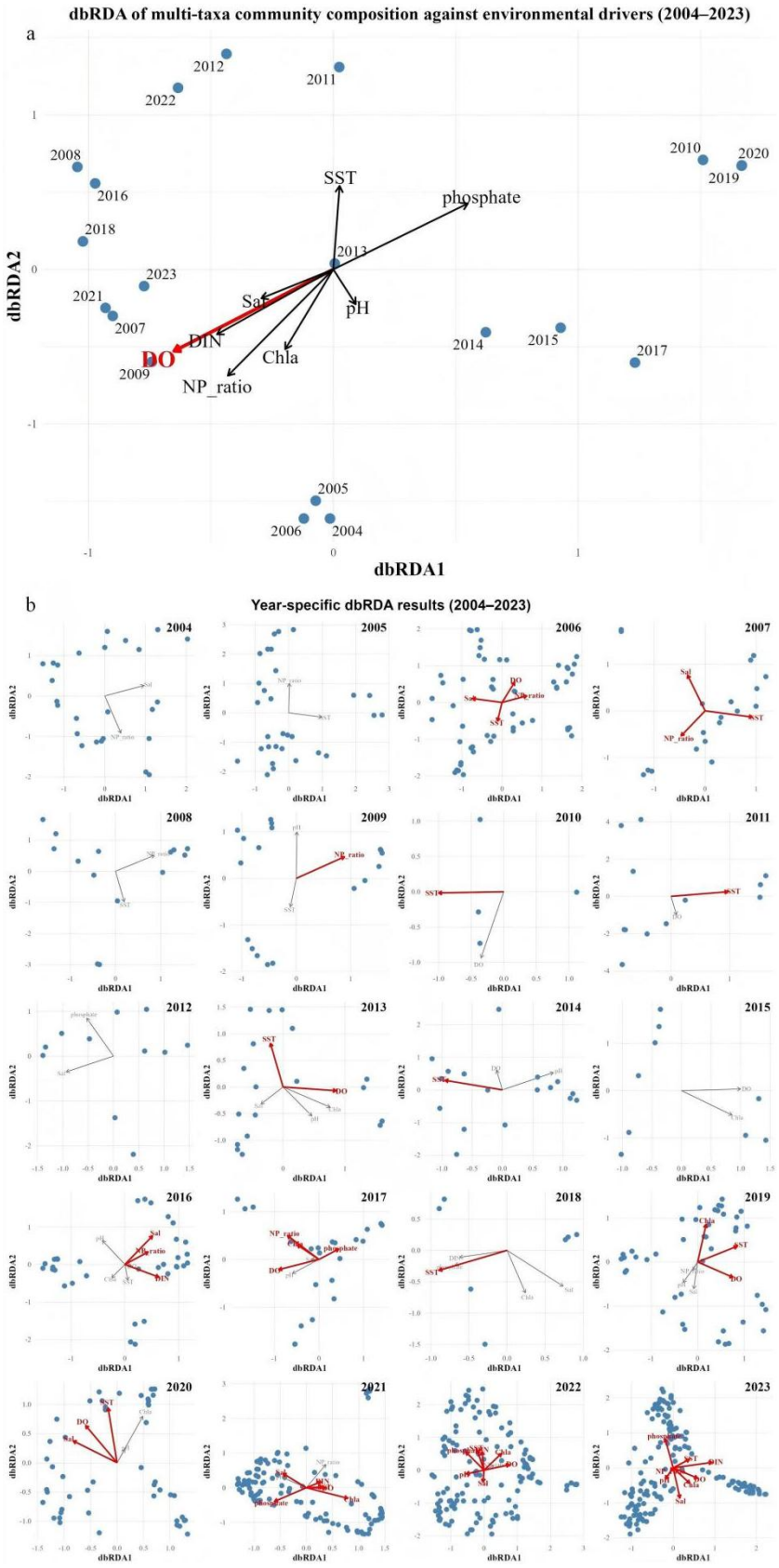


Fig. 3 | Distance-based redundancy analysis (dbRDA) results showing the influence of environmental variables on community composition across the four biotic groups.

a dbRDA biplot of community composition against environmental drivers at decade level. **b** Year-specific significant environmental drivers identified by dbRDA from 2004 to 2023. The length and direction of arrows indicate the strength and sign of each variable's correlation with community composition. Red cells indicate significant drivers ($p < 0.05$) while black cells indicate non-significant variables.

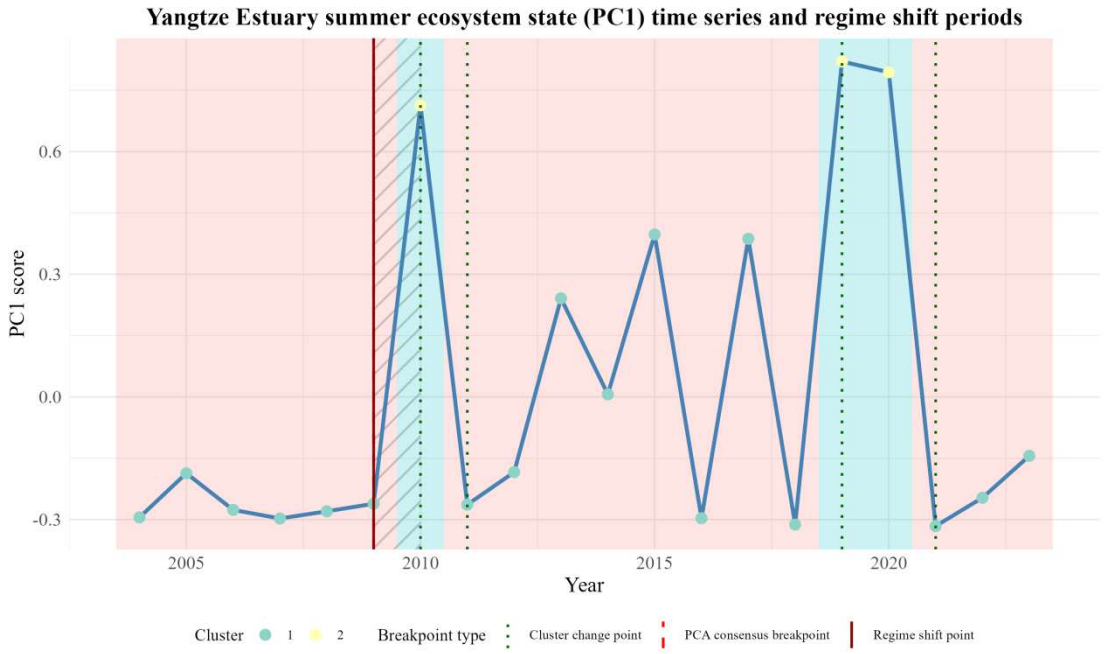


Fig. 4 | Identification of a multi-taxa regime shift in the Yangtze Estuary summer ecosystem, showing the convergence of PC1-based breakpoint detection and hierarchical clustering.

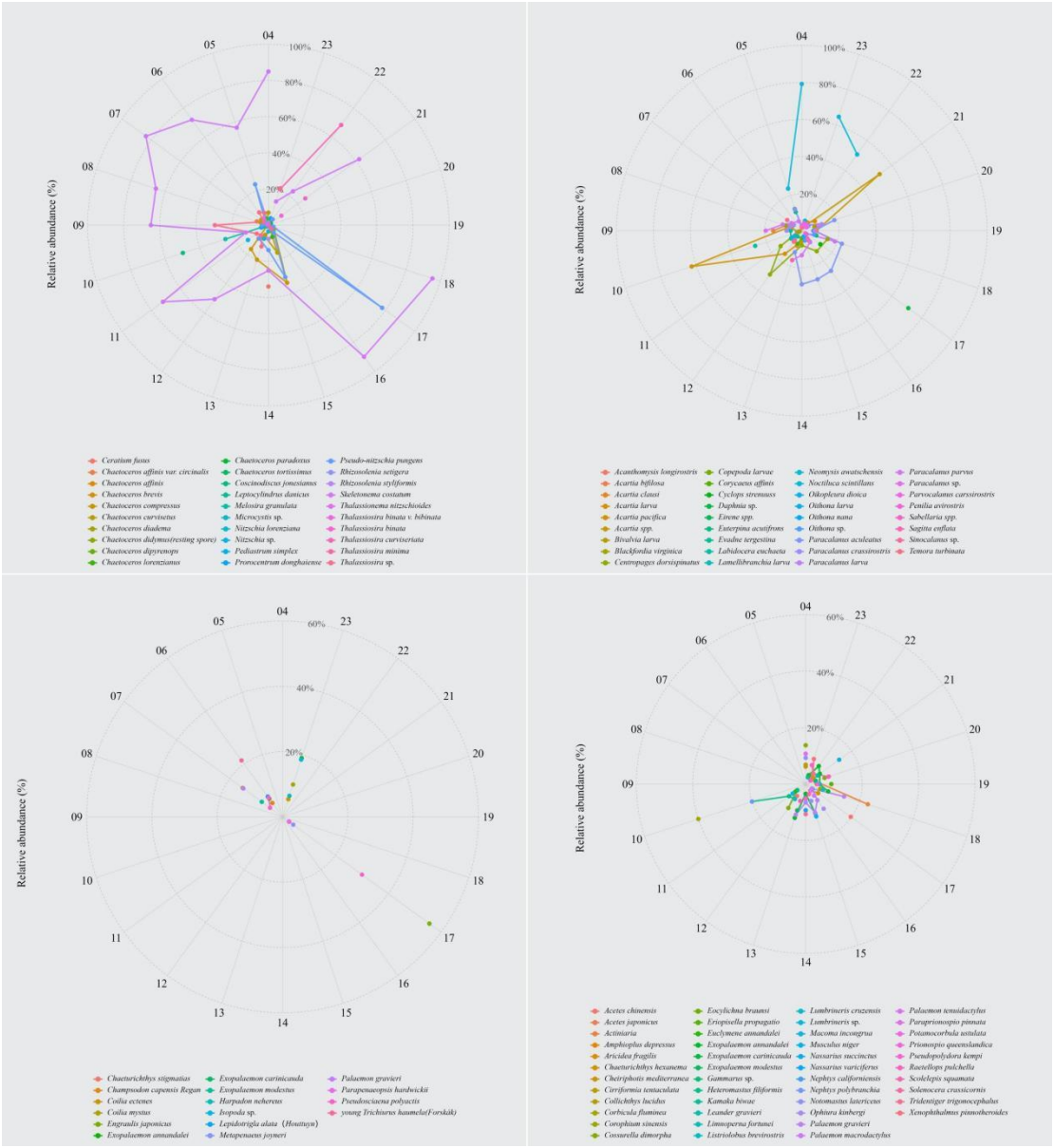


Fig. 5 | Changes in dominant species composition of each biotic group during summer before and after the regime shift in the Yangtze Estuary. a Phytoplankton. b Zooplankton. c Nekton. d Benthos.

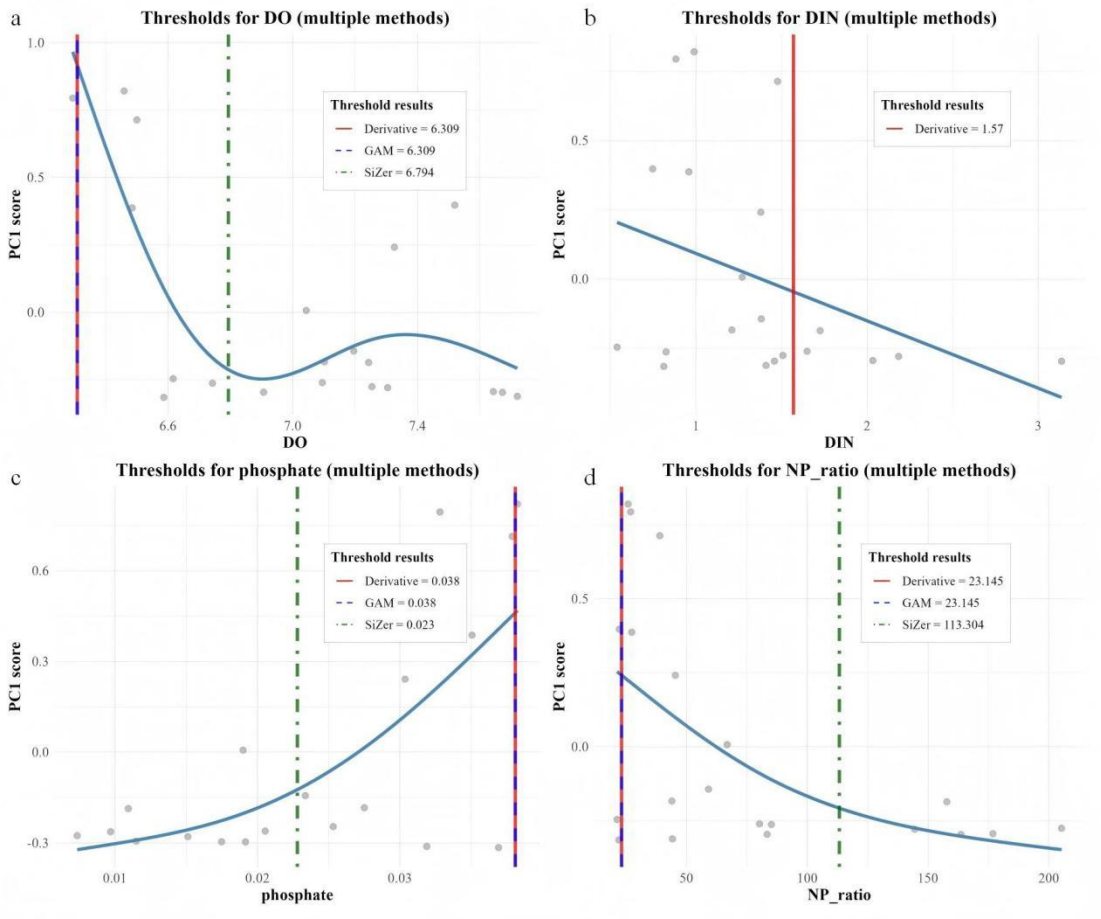


Fig. 6 | Threshold responses of PC1 to four significant environmental drivers, identified by the non-parametric derivative method with cross-validation from GAM-based permutation tests and the exploratory SiZer method.

a DO threshold identified by the derivative method and confirmed by GAM permutation, derived from the PC1-DO response curve, with a negative slope. **b** DIN threshold identified by the derivative method and consistent with GAM permutation, derived from the PC1-DIN response curve, with a negative slope, though SiZer detected no threshold. **c** Phosphate threshold identified by the derivative method and confirmed by GAM permutation, derived from the PC1-phosphate response curve, with a positive slope, while SiZer detected a lower value. **d** N/P threshold identified by the derivative method and consistent with GAM permutation, derived from the PC1-N/P response curve, with a negative slope, while SiZer detected a higher value.

Supplementary Files

This is a list of supplementary files associated with this preprint. Click to download.

- SupplementaryMaterial.docx
- SupplementaryMaterial.docx